Received: 17 January 2019 | Revised: 5 July 2019 | Accepted: 29 July 2019

DOI: 10.1111/gbi.12360

ORIGINAL ARTICLE

gebiology WILEY

A paleosol record of the evolution of Cr redox cycling and evidence for an increase in atmospheric oxygen during the Neoproterozoic

David Auerbach Colwyn[1] | Nathan D. Sheldon[2] | J. Barry Maynard[3] | Robert Gaines[4] | Axel Hofmann[5] | Xiangli Wang[1,6,7] | Bleuenn Gueguen[1,8] | Dan Asael[1] | Christopher T. Reinhard[9] | Noah J. Planavsky[1]

[1]Department of Geology and Geophysics, Yale University, New Haven, CT, USA

[2]Department of Earth and Environmental Sciences, University of Michigan, Ann Arbor, MI, USA

[3]Department of Geology, University of Cincinnati, Cincinnati, OH, USA

[4]Geology Department, Pomona College, Claremont, CA, USA

[5]Department of Geology, University of Johannesburg, Johannesburg, South Africa

[6]Department of Marine Sciences, University of South Alabama, Mobile, AL, USA

[7]Dauphin Island Sea Lab, Dauphin Island, AL, USA

[8]Institut Universitaire Européen de la Mer, CNRS UMS 3113, Université de Brest, Plouzané, France

[9]School of Earth and Atmospheric Sciences, Georgia Institute of Technology, Atlanta, GA, USA

Correspondence
David Auerbach Colwyn, Department of Geology and Geophysics, Yale University, New Haven, CT 06511, USA.
Email: david.colwyn@colorado.edu

Funding information
National Science Foundation; NASA Astrobiology Institute; Division of Earth Sciences, Grant/Award Number: 1050760

Abstract

Atmospheric oxygen levels control the oxidative side of key biogeochemical cycles and place limits on the development of high-energy metabolisms. Understanding Earth's oxygenation is thus critical to developing a clearer picture of Earth's long-term evolution. However, there is currently vigorous debate about even basic aspects of the timing and pattern of the rise of oxygen. Chemical weathering in the terrestrial environment occurs in contact with the atmosphere, making paleosols potentially ideal archives to track the history of atmospheric O_2 levels. Here we present stable chromium isotope data from multiple paleosols that offer snapshots of Earth surface conditions over the last three billion years. The results indicate a secular shift in the oxidative capacity of Earth's surface in the Neoproterozoic and suggest low atmospheric oxygen levels (<1% PAL pO_2) through the majority of Earth's history. The paleosol record also shows that localized Cr oxidation may have begun as early as the Archean, but efficient, modern-like transport of hexavalent Cr under an O_2-rich atmosphere did not become common until the Neoproterozoic.

KEYWORDS

atmospheric oxygenation, chromium isotopes, paleosol, redox

1 | INTRODUCTION

Atmospheric oxygenation played a critical role in the development of modern biogeochemical cycling (e.g., Goldblatt, Lenton, & Watson, 2006; Lenton & Daines, 2017a; Lyons, Fike, & Zerkle, 2015; Lyons, Reinhard, & Planavsky, 2014; Och & Shields-Zhou, 2012) and in the evolution of complex life (Canfield, Poulton, & Narbonne, 2007; Erwin et al., 2011; Knoll, Bergmann, & Strauss, 2016; Knoll & Sperling, 2014). The traditional view of atmospheric oxygen levels over geologic time has been that Earth underwent a unidirectional rise in surface oxygen levels. Multiple lines of evidence, foremost the rare sulfur isotope record (e.g., Farquhar, Bao, & Thiemens,

2000; Halevy, Johnston, & Schrag, 2010; Pavlov & Kasting, 2002; Reinhard, Planavsky, & Lyons, 2013), point to extremely low atmospheric pO_2 prior to a "Great Oxidation Event" (GOE) at ~2.4–2.3 Ga (e.g., Holland, 2006). This view has been reinforced by long-term records of redox-sensitive crustal trace elements such as chromium (e.g., Babechuk, Kleinhanns, & Schoenberg, 2017; Konhauser et al., 2011; Murakami, Matsuura, & Kanzaki, 2016; Reinhard, Planavsky, Robbins, et al., 2013; Robbins et al., 2016). Atmospheric oxygen levels are typically assumed to have risen to near-modern levels during the Neoproterozoic (Holland, 2006) or the Paleozoic with the rise of land plants (Lenton, Daines, & Mills, 2018; Wallace et al., 2017).

This broad stair-step view of Earth's oxygenation is supported by several lines of geological and geochemical evidence (e.g., Farquhar, Zerkle, & Bekker, 2011; Holland, 2006; Lyons et al., 2014). Recently, however, it has been recognized that atmospheric oxygen levels in the Precambrian may have been more dynamic than traditionally envisioned. For example, there have been multiple suggestions that the atmosphere saw pulses of oxygen well above the low background pO_2 in the roughly half-billion years leading up to the GOE (e.g., Anbar et al., 2007; Crowe et al., 2013; Kendall, Brennecka, Weyer, & Anbar, 2013). Atmospheric oxygen levels during these early "whiffs" may have been quite high, potentially exceeding 0.1% of present atmospheric oxygen levels (% PAL; e.g., Crowe et al., 2013, but c.f. Albut et al., 2018). Some of these signals for high atmospheric Archean oxygen levels have also been linked to localized oxygen production (e.g., within microbial mats; Lalonde & Konhauser, 2015). Atmospheric pO_2 may have also undergone significant fluctuations during the Proterozoic, rather than experiencing stasis or a unidirectional rise. Traditional estimates for Proterozoic atmospheric oxygen levels following the GOE range between 1% and 40% PAL, based on assumed retention of iron in paleosols, and the assumed presence of an anoxic deep ocean (Kump, 2008). However, this interpretation was based heavily on the 1.1 Ga Sturgeon Falls paleosol (Zbinden, Holland, Feakes, & Dobos, 1988), which has subsequently been found to exhibit iron and manganese loss instead of retention (Mitchell & Sheldon, 2009, 2010, 2016), an observation now repeated for at least two other penecontemporaneous paleosols (Planavsky et al., 2018).

The last decade of research has led to a more nuanced view of atmospheric pO_2, which recognizes that pO_2 may have risen to Phanerozoic-like levels in the Paleoproterozoic (Canfield, 2005; Lyons et al., 2014; Partin et al., 2013) and crashed to levels much lower than traditionally envisioned in the mid-Proterozoic (e.g., Bellefroid et al., 2018; Canfield, 1998; Cole et al., 2016; Crockford et al., 2018; Gilleaudeau et al., 2016; Hardisty et al., 2017; Li et al., 2015; Lyons et al., 2014; Planavsky et al., 2014; Scott et al., 2011; Tang, Shi, Wang, & Jiang, 2016). Evidence for inhibited Cr oxidation in the mid-Proterozoic (Cole, O'Connell, & Planavsky, 2018; Cole et al., 2016; Planavsky et al., 2014) also supports the case for low surface oxygen levels. However, the interpretation of empirical records as showing low mid-Proterozoic atmospheric oxygen levels has been questioned (Daines, Mills, & Lenton, 2017; Lenton & Daines, 2017a; Zhang et al., 2017). There are also several recent reports of high mid-Proterozoic atmospheric oxygen levels (Daines et al., 2017; Gilleaudeau et al., 2016; Zhang et al., 2016), although the robustness of these records and their interpretations has similarly been debated (e.g., Cole et al., 2016; Planavsky et al., 2016). Perhaps the only thing about Proterozoic oxygen levels that *is* very clear is that there is an ongoing debate, which raises an unequivocal need for new records of the past redox state of Earth's surface environment.

In order to provide a new view of atmospheric O_2 through time, we investigated a set of well-studied paleosols using stable chromium isotopes. Isotopic fractionation in the Cr isotope system occurs primarily during redox reactions (Ellis, Johnson, & Bullen, 2002). ^{52}Cr is preferentially retained compared to ^{53}Cr during manganese oxide-mediated oxidation of Cr(III) to Cr(VI), and the resulting Cr(VI) has a much higher solubility than Cr(III). Under oxidizing conditions, terrestrial weathering releases a dissolved solute load that is ^{53}Cr-enriched (e.g., Frei, Gaucher, Poulton, & Canfield, 2009). Beneath a well-oxygenated atmosphere, soils develop highly variable Cr isotope values, but on average, the weathered material is more depleted in ^{53}Cr than the crustal inventory (Schoenberg, Zink, Staubwasser, & Von Blanckenburg, 2008) because of extensive Cr(III) oxidation and subsequent loss of ^{53}Cr-enriched Cr(VI) species. Isotope mass balance is maintained via the removal of ^{53}Cr to rivers and eventually the oceans, where marine sedimentary rocks can capture this mobile, ^{53}Cr-enriched signal (Cole et al., 2016; Frei et al., 2009; Gueguen et al., 2016; Reinhard et al., 2014). The sensitivity of stable Cr isotopes to oxidative weathering makes Cr isotopes useful redox tracers, particularly in the oxidant-poor Precambrian (e.g., Crowe et al., 2013; Frei et al., 2009; Planavsky et al., 2014). Importantly, developing large negative Cr isotope signals in paleosols can be linked to transport of oxidized Cr out of the paleosol, which will be limited in the presence of hexavalent Cr reductants (foremost Fe^{2+}).

Recently work produced evidence for significant Cr isotope fractionations during Cr(III) complexation with simple ligands during inorganic and organic complexation (Babechuk, Kleinhanns, Reitter, & Schoenberg, 2018; Saad, Wang, Planavsky, Reinhard, & Tang, 2017), which adds an additional complication to the Cr isotope system. Saad et al. (2017) noted that the fractionations observed during these interactions are variable in magnitude, with the implication that they are unlikely to cause a coherent shift in the mean value of the soil Cr isotope reservoir. However, on longer time scales, Cr(III)-organic ligand complexes investigated thus far are uniformly ^{52}Cr-enriched (Saad et al., 2017), and inorganic complexes appear to behave similarly (Babechuk et al., 2018). This implies that coupled ligand-Cr cycling in weathering environments should lead to preferential export of isotopically light Cr. So while ligand interactions add important mechanistic detail to the framework for interpreting Cr isotopes, strongly weathered soils with sub-crustal Cr isotope values provide the most direct Cr isotope signal for a well-oxygenated surface environment (Crowe et al., 2013; Frei et al., 2009).

TABLE 1 Summary of paleosol localities and age constraints

Paleosol name & location	Age (Ga)	Parent material & lower age constraint	Upper age constraint	References
Basal Pongola paleosol Mpumalanga, South Africa	3.0	Developed on Archean felsic gneisses and intruding plutonic rocks (incl. granodiorites) with zircon U-Pb ages as young as 3,105 ± 3 Ma	Overlain by Nsuze Group, which includes bad-deleyite U-Pb ages as old as 2,978 ± 2 Ma and zircon U-Pb ages as old as 2,980 ± 10 Ma	Grandstaff, Edelman, Foster, Zbinden, and Kimberley (1986); Kimberley and Grandstaff (1986); Mukasa, Wilson, and Young (2013); Wilson and Zeh (2018)
Nsuze (Denny Dalton) paleosol KwaZulu-Natal, South Africa	2.96	Developed on basaltic andesite of the Nsuze Group, which includes a zircon U-Pb date of 2,968 ± 6 Ma	Overlain by Mozaan Group, which contains zircon U-Pb ages as old as 2,954 ± 9 Ma	Crowe et al. (2013); Wilson and Zeh (2018); Delvigne, Opfergelt, Cardinal, Hofmann, and André (2016)
Saganaga paleosol Minnesota, USA	2.685	Developed on Saganaga to-nalite with zircon U-Pb age of 2,690.83 ± 0.26 Ma	Overlain by conglomerate of the Ogishkemuncie se-quence which was deformed at ~ 2,680 Ma	Driese et al. (2011)
Cooper Lake paleosol Ontario, Canada	2.45	Developed on diabase of the Thessalon Fm. & sandstone of the Livingstone Creek Fm. Thessalon Fm. lavas yield a zircon U-Pb age of 2,452.5 ± 6.2 Ma; Livingstone Creek Fm. detrital zircons have a young peak at ~ 2,675 Ma	Overlain by Matinenda Fm., which contains a youngest detrital zircon population of ~ 2,475 Ma and is over-lain by tuffs in Gordon Lake Fm. with a U/Pb zircon age of 2,308 ± 8 Ma	Sutton and Maynard (1993); Rye and Holland (1998); Prasad and Roscoe (1991); Utsunomiya, Murakami, Nakada, and Kasama (2003); Krogh, Davis, and Corfu (1984); Ketchum, Heaman, Bennett, and Hughes (2013); Rasmussen, Bekker, and Fletcher (2013); Babechuk et al. (2019)
Lauzon Bay paleosol Ontario, Canada	2.45	Developed on ~ 2.5 Ga Algoman granite	Overlain by Matinenda Fm., which contains a youngest detrital zircon population of ~ 2,475 Ma and is over-lain by tuffs in Gordon Lake Fm. with a U/Pb zircon age of 2,308 ± 8 Ma	Prasad and Roscoe (1991); Sutton and Maynard (1992); Maynard et al. (2013); Krogh, Davis, and Corfu (1984; Rasmussen, Bekker, and Fletcher (2013); Babechuk et al. (2019)
Mid-Continent Rift paleosols (Two Harbors & Pike Lake Road, Minnesota, USA)	1.1	Developed on tholeiitic basalt within the 1,108–1,094 Ma North Shore Volcanic Group	Overlain by 1,097 ± 2 Ma Palisade Head Rhyolite	Green and Fitz (1993); Ojakangas, Morey, and Green (2001); Mitchell and Sheldon (2009, 2010, 2016)
Verde River paleosol Arizona, USA	0.52	Developed on basalts of the Payson Ophiolite, which includes a zircon U-Pb date of 1,729 ± 6 Ma	Continuously overlain by fluvial sandstones of the Early Cambrian Tapeats Sandstone	Dann, Chamberlain, and Bowring (1989, 1991, 1997); Supporting Information
St. Francois Mountains paleosol Missouri, USA	0.50	Developed on 1.4–1.3 Ga granitic rocks	Overlain by Late Cambrian Lamotte Sandstone	Sutton and Maynard (1996)
Olive Hill Clay paleosol Kentucky, USA	0.323	Developed on shale of the upper Mississippian Pennington, Borden, & Newman Fms	Overlain by Lower Pennsylvanian Lee & Breathitt Fms	Smyth (1984)

1.1 | Paleosols

We measured Cr isotope profiles in 10 paleosols (Table 1), nine which are previously described and the Verde River paleosol, which we describe here (see Supporting Information). These paleosols span a range of ages from Mesoarchean (3.0 Ga, in the Pongola Supergroup of South Africa) to Carboniferous (0.323 Ga, from Kentucky, USA). Precambrian paleosols have often been marked by controversy over their identification as well as the fidelity of their geochemistry (see for instance discussion in Tarhan et al., 2018). This has been discussed in detail, most notably by Rye and Holland (1998), who stressed that well-preserved paleosols should fulfill a series of criteria regarding their parent rock, texture, mineralogy, and geochemistry. This is particularly important in Precambrian paleosols, which are more likely to have been subjected to diagenesis or alteration of the parent rock, burial metasomatism, and/or metamorphism. Consequently,

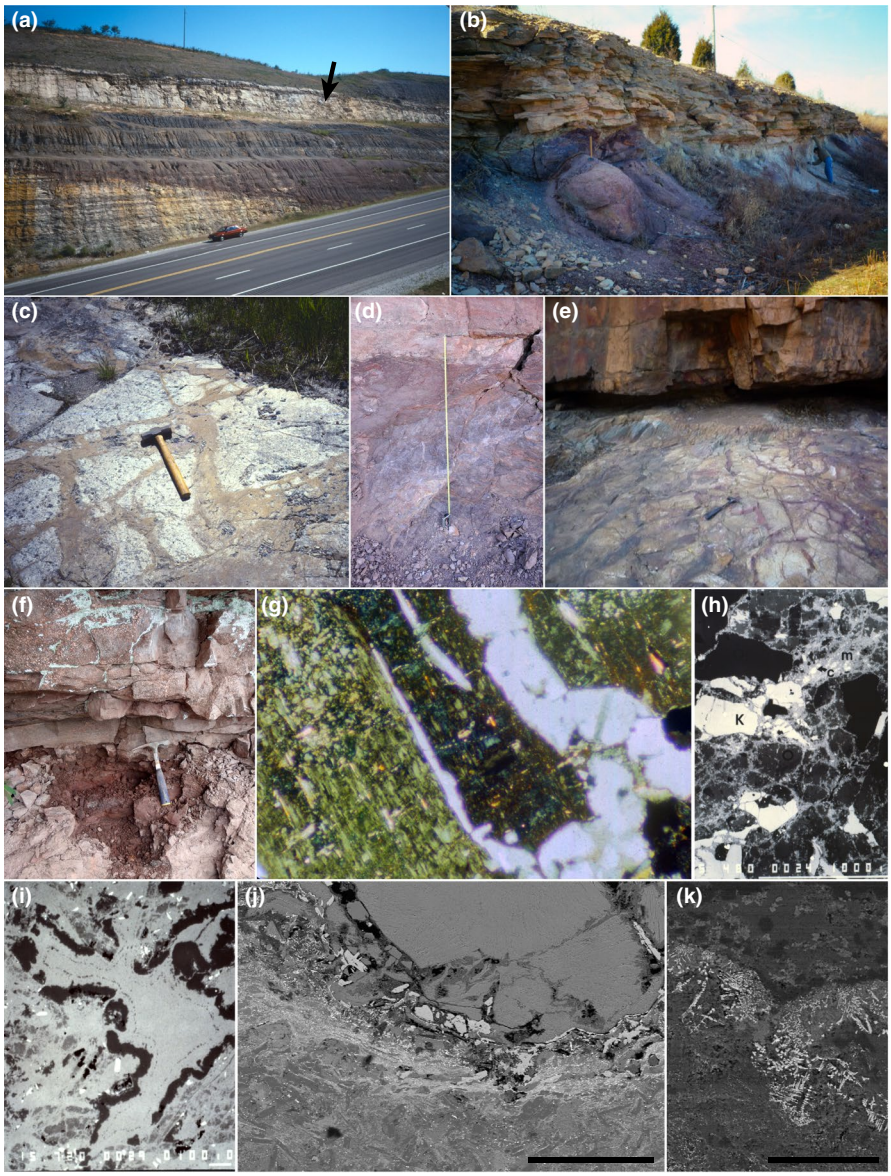

FIGURE 1 Representative depictions of paleosols in outcrop, thin section, and SEM images. (a) Outcrop of 0.323 Ga Olive Hill Clay paleosol along Kentucky State Highway AA. Paleosol is the conspicuous light-colored unit between lower and upper black shales (denoted by arrow). Automobile for scale. (b) ca. 0.5 Ga St. Francois Mountains paleosol in outcrop, showing granitic corestones. Overlying rock is the Upper Cambrian Lamotte Sandstone. 40-cm-long rock hammer rests on paleosol top. (c) 2.45 Ga Lauzon Bay paleosol with remnant corestones of granite parent rock. 40-cm-long rock hammer for scale. (d) Dark-colored ca. 0.54 Ga Verde River paleosol in outcrop, sharply overlain by light-colored fluvial sandstones of the Lower-Middle Cambrian Tapeats Fm. (e) 2.96 Ga Nsuze paleosol, showing spheroidal weathering in the paleosol, which is overlain by sedimentary rocks of the Mozaan Group. 30-cm-long rock hammer for scale. (f) 1.1 Ga Two Harbors paleosol, exposed near Two Harbors, MN. (g) Thin section of St. Francois Mountains paleosol (3 m below top), showing weathered feldspars. Field of view is 1.77 mm across. (h) BSE image of the Lauzon Bay paleosol (2.5 m below top), showing weathered minerals of parent granite. K = K-feldspar, O = oligoclase, m = mica, c = chlorite. Scale bar is 0.5 mm. (i) BSE image of weathered feldspar in 2.45 Ga Cooper Lake diabase (2 m below top). Scale bar is 100 μm. (j) Pike Lake Road paleosol. BSE image shows weathering of a Fe-rich pyroxene grain. Scale bar is 200 μm. (k) BSE image of Pike Lake Road paleosol, showing development of dendritic Fe-oxide minerals along the margin of weathered pyroxene. Scale bar is 50 μm

we limited our work to paleosols that have been studied in detail and fit the mineralogical, textural, and geochemical criteria that establish them as definitive paleosols (Rye & Holland, 1998; see Figure 1, Supporting Information) and have relatively low metamorphic grades. Furthermore, we have limited our study to paleosols developed on igneous rocks (with the exception of the Olive Hill paleosol and the Cooper Lake "quartzite"), to facilitate comparison and to minimize weathering prior to paleosol development.

Preservation of Precambrian paleosols is rare (e.g., Holland & Zbinden, 1988; Rye & Holland, 1998). Precambrian paleosols that are preserved and ultimately identified are often not typical weathering profiles; the Precambrian paleosols that we

investigated are typically several meters to tens of meters thick. These paleosols likely represent extended periods of weathering (Table 1, Supporting Information), although poor constraints on soil-forming conditions (e.g., climate, biotic activity, relief, time; see Jenny, 1941) in the Precambrian make it difficult to definitively establish the time span represented by these paleosols. Perhaps the most analogous modern soils are the old, thick, intensely weathered soil profiles of the Amazon region, which have high weathering indices (e.g., CIA-K) and are meters to tens of meters thick. Appropriate Phanerozoic analogs include the thick paleosols that often mark sedimentary sequence boundaries (e.g., DeCelles, Carrapa, Horton, & Gehrels, 2011). Even if these paleosols are only of moderate (kyr) duration, the time span of weathering that forms paleosols produces ideally time-averaged records of chemical weathering under contemporaneous atmospheric conditions (e.g., Sheldon, 2006).

2 | METHODS

Our method for Cr isotope analysis closely follows that of Schoenberg et al. (2008). Sample powders were drilled from fresh samples taken either from outcrop or core. Powdered paleosol samples were weighed, ashed at 500°C, and then digested at 90°C using a series of acid dissolution steps used widely (e.g., Babechuk et al., 2017; D'Arcy, Babechuk, Døssing, Gaucher, & Frei, 2016; Frei et al., 2009) to prepare silicate samples for Cr isotope analysis: HF + HNO_3, aqua regia, and finally 6N HCl. This digest protocol is considered sufficient to liberate all Cr in spinel-free rocks (such as the ones studied here) save for the minor Cr in zircon; the similarity of the digestion procedure to other laboratories also facilitates direct comparison of isotope data. Elemental concentrations were determined on aliquots of dissolved sample diluted in 5% HNO_3 using a Thermo Scientific Element-XR ICP-MS at Yale Metal Geochemistry Center or on an Agilent 7700X ICP-MS in the Trace Element Analysis laboratory at Dartmouth College. The purification procedure, analytical protocol, and data reduction follow the methods of Gueguen et al. (2016). An aliquot of each sample was collected and spiked with a ^{50}Cr-^{54}Cr double-spike at a $^{54}Cr_{spike}/^{52}Cr_{sample}$ ratio of ~0.5 and purified using ion exchange chromatography columns. The purified Cr was analyzed on a Thermo Scientific Neptune Plus MC-ICP-MS at Yale Metal Geochemistry Center with correction for potential interferences from Fe, V, and Ti. Chromium isotope ratios (Table 2) are reported relative to standards using conventional delta notation, where $\delta^{53}Cr = [(^{53}Cr/^{52}Cr)_{sample}/(^{53}Cr/^{52}Cr)_{SRM979} - 1] \times 1{,}000$ and is thus expressed per mil (‰). Precision was better than 0.11‰ (2SE), based on duplicate analyses of geological reference materials BHVO-2 (basalt) and Nod-A-1 (Mn nodule). Our measured $\delta^{53}Cr$ values for these standards—BHVO-2 = −0.19 ± 0.08‰ (2*SD*, *n* = 7); Nod-A-1 = 0.04 ± 0.03‰ (2*SD*, *n* = 7)—match well with previous studies using the same digestion procedure on standards that match the type of samples analyzed (Gueguen et al., 2016; Schoenberg et al., 2008; Wang et al., 2016).

3 | RESULTS

3.1 | Cr isotope geochemistry

The paleosol $\delta^{53}Cr$ data (Figure 2, Table 2) provide a 3.0 Gyr record of terrestrial environmental conditions. The primary pattern in the data is the general absence of sub-crustal $\delta^{53}Cr$ values from ca. 3.0 to 1.1 Ga, where the crustal (bulk silicate Earth) array is defined as $\delta^{53}Cr$ = −0.124 ± 0.101‰ (Schoenberg et al., 2008; Wang et al., 2016). During that interval, the $\delta^{53}Cr$ value is either crustal or supra-crustal ($\delta^{53}Cr$ = 0.48 to −0.28‰). The exception is the 2.96 Ga Nsuze paleosol, which includes values as low as −0.37‰. This is the same paleosol analyzed by Crowe et al. (2013), who report values as low as −0.98 ± 0.12‰ from samples at a different location (although Albut et al. (2018) suggest those low values may be a modern weathering overprint). Our $\delta^{53}Cr$ data from Cooper Lake are similar to those recently reported by Babechuk et al. (2019). The 1.1 Ga Pike Lake Road and Two Harbors paleosols formed at close but not identical points in space and time (<50 km and <15 Myr, likely much less time based on sedimentological observations), and their similar values (0.48‰ to −0.27‰ vs. 0.32‰ to −0.15‰) reinforce the robust nature of these data. After ~0.6 Ga, the appearance of sub-crustal values becomes the rule rather than the exception, beginning with the late Neoproterozoic–Cambrian Great Unconformity paleosol from Verde River. The range of values observed in these paleosols (~0.5‰ to −0.6‰) is similar to the range observed in the Carboniferous Olive Hill paleosol as well as previously described Cretaceous, Cenozoic, and modern soil profiles (Figure 2; Berger & Frei, 2014; D'Arcy et al., 2016; Frei, Poiré, & Frei, 2014; Wang et al., 2016; Wille et al., 2018). In contrast, the St. Francois Mountains paleosol shows $\delta^{53}Cr$ values that are largely confined to the crustal range. The fact that two nearly contemporaneous paleosols (Verde River and St. Francois Mountains) have very different ranges is not surprising given the potential spatial variability in redox and soil forming conditions (e.g., precipitation, temperature). Alternatively, it could also reflect input of allochthonous material to the St. Francois Mountains paleosol (see below) or lower surface oxygen levels (a more weakly buffered system) than was present later in the Phanerozoic.

We grouped the paleosol $\delta^{53}Cr$ data (Figure 2) into three time intervals—the Archean and early Paleoproterozoic (3.0–2.45 Ga), the mid-Proterozoic (ca. 1.1 Ga), and the end-Proterozoic and Phanerozoic (<0.6 Ga; Figure 3). From the Archean through the mid-Proterozoic (3.0–1.1 Ga), the data are distributed over a narrow range of values—largely in the crustal range—and have non-normal distributions (Table S1). Between 1.1 and ca. 0.6 Ga, the variance of the data increases and the range and distribution become more normal, similar to modern (Figure 3, Table S1).

TABLE 2 Geochemical data from paleosol profiles. Column entitled "Method" indicates the analytical technique used to measure the elemental abundances. Italicized rows indicate samples used as parent for mass balance calculations (Table 3)

Paleosol	Age (Ga)	Depth below top[a] (m)	Cr (ppm)	$\delta^{53/52}$Cr (‰)	2SE (‰)	Fe (%)	Al (%)	Ti (%)	V (ppm)	Method	Cr/Ti	Cr/Al	Al/Ti	$\tau(i,j)$ for (Al,Cr)
Basal Pongola	3.0	0.08	43.14	−0.06	±0.03	5.70	1.14	0.04	11.0	ICP-MS	0.0976	0.00380	25.69	0.00
		2.6	139.99	−0.03	±0.02	4.66	3.32	0.16	41.0		0.0890	0.00422	21.10	0.12
		2.6	131.31	−0.07	±0.03	4.67	3.15	0.16	38.3		0.0843	0.00417	20.22	0.79
		2.8	43.12	−0.05	±0.03	7.23	0.64	0.04	7.8		0.1231	0.00678	18.14	0.10
		2.8	*53.86*	*−0.08*	*±0.03*	*4.74*	*1.42*	*0.05*	*11.8*		*0.1088*	*0.00378*	*28.75*	
Nsuze (Denny Dalton)	2.96	0.4	80.98	−0.24	±0.03	0.27	5.59	0.53	202.4	ICP-MS	0.0153	0.00145	10.53	0.43
		0.7	63.40	−0.25	±0.02	0.21	5.46	0.45	153.7		0.0141	0.00116	12.17	0.15
		0.95	52.45	−0.30	±0.02	0.23	5.87	0.40	134.9		0.0132	0.00089	14.77	−0.12
		2.15	46.74	−0.30	±0.02	5.04	4.27	0.15	120.6		0.0319	0.00109	29.17	0.08
		3.45	20.60	−0.29	±0.03	6.00	2.59	0.10	48.4		0.0202	0.00080	25.29	−0.21
		4.35	23.60	−0.24	±0.02	6.28	2.79	0.12	57.2		0.0206	0.00085	24.39	−0.16
		5.45	27.01	−0.24	±0.02	5.91	3.15	0.10	65.9		0.0269	0.00086	31.41	−0.15
		10	56.14	−0.26	±0.02	4.42	2.55	0.08	52.3		0.0698	0.00220	31.74	1.18
		15	*36.06*	*−0.31*	*±0.02*	*5.51*	*3.57*	*0.07*	*75.3*		*0.0523*	*0.00101*	*51.68*	
Saganaga	2.865	−6	68.95	0.26	±0.02	1.71	7.71	0.15	42.3	XRF &	0.0474	0.00089	52.97	
		−1.5	83.77	0.06	±0.04	1.80	7.84	0.16	47.5	ICP-AES/	0.0538	0.00107	50.32	
		0	78.76	−0.13	±0.05	1.86	7.50	0.14	45.9	ICP-MS[b]	0.0566	0.00105	53.83	0.45
		0.3	64.48	0.09	±0.05	0.86	8.96	0.21	43.0		0.0313	0.00072	43.46	−0.01
		18	62.93			0.62	8.26	0.17	37.5		0.0369	0.00076	48.36	0.05
		46	*45.24*	*0.26*	*±0.05*	*0.71*	*5.94*	*0.14*	*31.8*		*0.0332*	*0.00076*	*43.56*	
		49	*33.12*	*0.07*	*±0.02*	*0.68*	*4.57*	*0.12*	*26.9*		*0.0285*	*0.00072*	*39.35*	
		55	*51.95*	*0.04*	*±0.04*	*1.28*		*0.13*	*43.7*		*0.0412*			
Lauzon Bay	2.45	−0.5	4.77	−0.09	±0.03	0.21	2.48	0.02	6.2	ICP-MS	0.0291	0.00019	151.21	
		−0.2	3.47	−0.09	±0.03	0.11	1.66	0.01	3.2		0.0293	0.00021	140.54	
		0	3.40	−0.15	±0.03	0.34	3.66	0.06	5.9		0.0057	0.00009	61.00	−0.91
		0.4	1.50	−0.22	±0.03	0.25	3.51	0.03	3.4		0.0056	0.00004	132.16	−0.96
		1.4	2.02	−0.20	±0.03	0.23	2.62	0.02	4.1		0.0084	0.00008	109.39	−0.92
		2.1	3.56	−0.11	±0.02	0.33	3.76	0.02	4.8		0.0156	0.00009	164.18	−0.91
		3.5	2.66	−0.13	±0.03	0.23	2.67	0.03	3.2		0.0107	0.00010	106.81	−0.90
		4.5	3.22	−0.11	±0.02	0.30	3.20	0.03	4.5		0.0112	0.00010	111.60	−0.90
		6.5	*3.38*	*−0.18*	*±0.03*	*0.36*	*2.99*	*0.03*	*3.7*		*0.0111*	*0.00011*	*98.70*	
Cooper Lake[c]	2.45	0.5	2.39	−0.21	±0.02	0.27	2.36	0.04	1.3	ICP-MS	0.0274	0.00033	66.43	−0.36
		2.5	4.97	−0.16	±0.02	0.10	1.20	0.02	2.7		0.0302	0.00044	55.82	−0.14
		3.5	6.70	−0.12	±0.02	0.11	1.14	0.02	2.9		0.0318	0.00056	69.13	0.10
		4.5	9.95	−0.10	±0.02	0.08	0.50	0.01	4.5		0.0280	0.00042	69.78	−0.17
		6.5	*2.55*	*−0.28*	*±0.02*	*0.03*	*0.73*	*0.01*	*1.1*		*0.0354*	*0.00051*	*84.14*	
		0.75	1.27	−0.25	±0.02	1.38	4.27	0.42	255.0		0.0003	0.00003	10.11	
		3.0	1.47	−0.23	±0.02	5.09	2.31	0.23	132.9		0.0007	0.00006	10.24	
Two Harbors	1.1	−0.4	98.82	0.18	±0.02	8.21	9.38	0.84	250.7	ICP-AES/	0.0118	0.00105	11.15	
		0.05	111.22	−0.14	±0.02	6.55	10.22	0.82	217.2	ICP-MS[d]	0.0136	0.00109	12.48	−0.32
		0.1	106.53	−0.27	±0.02	6.30	10.34	0.80	214.0		0.0133	0.00103	12.89	−0.36
		0.35	131.27	0.18	±0.03	7.47	7.76	0.92	233.2		0.0142	0.00169	8.41	0.05
		0.35	93.52	0.05	±0.02	6.23	8.80	0.91	183.7		0.0103	0.00106	9.70	−0.34
		0.6	102.84	0.48	±0.03	8.16	6.39	0.88	274.8		0.0117	0.00161	7.29	0.00
		1	*114.64*	*−0.01*	*±0.04*	*8.14*	*8.25*	*0.85*	*252.4*		*0.0135*	*0.00139*	*9.68*	
Pike Lake Road	1.1	−0.4	37.27	−0.06	±0.02	9.04	6.77	1.26	256.8	ICP-AES/	0.0030	0.00055	5.36	
		0.2	67.54	−0.16	±0.02	6.35	6.75	0.44	117.2	ICP-MS[d]	0.0155	0.00100	15.46	−0.22
		0.2	51.42	−0.05	±0.02	6.52	6.20	0.70	141.8		0.0074	0.00083	8.90	−0.35
		0.3	99.25	−0.04	±0.02	6.61	8.11	0.64	131.0		0.0155	0.00122	12.67	−0.04
		0.42	57.76	0.09	±0.02	7.14	7.76	0.94	164.3		0.0061	0.00074	8.26	−0.42

(Continues)

TABLE 2 (Continued)

Paleosol	Age (Ga)	Depth below top[a] (m)	Cr (ppm)	$\delta^{53/52}$Cr (‰)	2SE (‰)	Fe (%)	Al (%)	Ti (%)	V (ppm)	Method	Cr/Ti	Cr/Al	Al/Ti	$\tau(i,j)$ for (Al,Cr)
		0.45	114.57	0.24	±0.02	6.06	8.09	0.67	132.4		0.0172	0.00142	12.13	0.63
		0.45	97.30	0.17	±0.02	6.95	7.62	0.64	171.5		0.0153	0.00128	11.94	0.11
		0.5	*118.74*	*0.32*	*±0.03*	*4.95*	*5.70*	*0.72*	*167.5*		*0.0165*	*0.00208*	*7.93*	
		0.55	*114.02*	*0.04*	*±0.03*	*6.41*	*8.04*	*0.73*	*179.6*		*0.0156*	*0.00142*	*11.01*	
Verde River	ca. 0.52	0.005	41.80	−0.30	±0.02	0.97	14.72	0.59	175.5	ICP-MS	0.0070	0.00028	24.80	−0.33
		0.01	60.50	−0.35	±0.03	0.64	15.33	0.58	150.4		0.0105	0.00039	26.64	−0.07
		0.025	64.60	0.26	±0.02	0.78	13.95	0.43	149.1		0.0152	0.00046	32.78	0.09
		0.03	57.90	0.47	±0.02	0.69	12.27	0.32	120.9		0.0182	0.00047	38.63	0.11
		0.05	52.50	0.09	±0.03	1.24	15.50	0.64	179.7		0.0083	0.00034	24.39	−0.20
		0.06	56.00	0.04	±0.02	1.30	14.87	0.56	173.0		0.0100	0.00038	26.67	−0.11
		0.07	56.50	0.20	±0.02	1.30	13.83	0.55	197.1		0.0104	0.00041	25.35	−0.04
		0.08	75.00	0.80	±0.07	0.92	13.06	0.53	183.4		0.0141	0.00057	24.48	0.35
		0.09	188.80	0.03	±0.03	0.64	15.26	0.65	171.7		0.0292	0.00124	23.57	1.92
		0.25	42.90	−0.20	±0.04	0.72	10.90	0.48	240.6		0.0089	0.00039	22.73	−0.07
		0.30	40.70	−0.15	±0.03	1.11	9.00	0.34	262.7		0.0121	0.00045	26.82	0.07
		0.50	26.30	−0.64	±0.02	0.71	8.91	0.41	225.4		0.0065	0.00030	21.85	−0.30
		0.50	28.70	−0.43	±0.03	7.48	5.49	0.42	235.8		0.0068	0.00052	13.08	0.21
		0.50	45.70	−0.20	±0.02	0.87	8.94	0.34	238.2		0.0134	0.00051	26.16	0.23
		0.50	49.91	−0.19	±0.03	8.81	6.86	0.37	260.8		0.0136	0.00073	18.75	0.72
		0.60	32.90	−0.38	±0.02	0.77	8.76	0.32	280.9		0.0104	0.00038	27.58	0.12
		0.70	60.20	−0.20	±0.02	0.55	8.02	0.28	197.2		0.0218	0.00075	29.08	0.77
		0.80	29.50	−0.18	±0.02	0.64	9.43	0.31	226.1		0.0097	0.00031	30.85	−0.26
		1.0	35.80	−0.15	±0.02	0.66	9.81	0.29	220.2		0.0122	0.00036	33.40	−0.14
		1.6	*54.60*	*−0.17*	*±0.02*	*0.68*	*9.42*	*0.32*	*217.8*		*0.0172*	*0.00058*	*29.63*	
		2.8	*29.60*	*−0.25*	*±0.03*	*0.63*	*8.71*	*0.28*	*193.7*		*0.0107*	*0.00034*	*31.58*	
St. Francois Mountains	ca. 0.50	0.0	3.15	−0.21	±0.03	0.40	3.92	0.09	21.1	ICP-MS	0.0036	0.00008	44.19	−0.31
		0.5	9.80	−0.16	±0.02	0.68	5.50	0.20	30.9		0.0048	0.00018	26.91	0.52
		1.0	3.91	−0.01	±0.02	0.81	7.60	0.09	26.9		0.0045	0.00005	87.61	−0.56
		1.5	3.85	−0.13	±0.02	0.37	4.82	0.11	21.1		0.0036	0.00008	45.55	−0.32
		2.0	1.96	−0.17	±0.04	0.56	6.82	0.07	20.0		0.0030	0.00003	103.04	−0.75
		2.5	4.44	−0.14	±0.02	0.53	6.06	0.12	21.8		0.0037	0.00007	50.01	−0.38
		15.0	*6.70*	*−0.14*	*±0.03*	*0.35*	*5.71*	*0.03*	*17.81*		*0.0195*	*0.00012*	*166.04*	
Olive Hill	0.323	0.01	263.58	−0.43	±0.02	7.19	19.54	1.89	302.3	ICP-MS	0.0140	0.00135	10.35	−0.01
		0.2	209.28	−0.57	±0.02	1.41	19.88	1.52	187.8		0.0138	0.00105	13.11	−0.23
		0.3	167.53	−0.24	±0.03	1.30	18.78	1.19	175.2		0.0141	0.00089	15.82	−0.35
		1	175.43	−0.61	±0.05	7.50	16.73	0.91	188.2		0.0193	0.00105	18.43	−0.23
		2.2	198.40	−0.45	±0.03	6.41	17.89	1.14	280.4		0.0175	0.00111	15.73	−0.19
		2.2	204.91	−0.46	±0.06	6.67	18.65	1.26	293.6		0.0163	0.00110	14.84	−0.19
		3.5	189.26	0.21	±0.03	5.54	17.72	0.92	203.8		0.0206	0.00107	19.32	−0.22
		4.0	175.30	0.30	±0.04	5.60	16.50	0.61	244.3		0.0288	0.00106	27.14	−0.22
		5.0	129.03	0.26	±0.02	5.13	13.23	0.47	213.5		0.0276	0.00098	28.29	−0.29
		6.0	109.44	0.23	±0.03	0.72	12.40	0.58	158.8		0.0189	0.00088	21.42	−0.35
		8.5	65.54	0.03	±0.02	1.27	5.04	0.36	103.6		0.0181	0.00130	13.94	−0.05
		8.8	*80.66*	*0.19*	*±0.02*	*1.26*	*5.21*	*0.44*	*121.8*		*0.0184*	*0.00155*	*11.89*	
		9.0	*75.44*	*0.15*	*±0.02*	*1.40*	*5.44*	*0.42*	*103.3*		*0.0178*	*0.00139*	*12.83*	
		10.0	*65.80*	*0.13*	*±0.02*	*0.89*	*4.91*	*0.40*	*119.5*		*0.0164*	*0.00134*	*12.20*	

[a]Negative numbers indicate samples from overlying rock.
[b]Major/minor elements by XRF, trace elements cross-checked on ICP-AES and ICP-MS.
[c]All samples within 1 m of each other; surface of weathering profile was not accessible.
[d]Elements cross-checked on ICP-AES and ICP-MS.

Paleosol name	Age (Ga)	Depth-weighted total $\tau_{i,j}$	Estimated δ^{53}Cr change (‰)	Restored original δ^{53}Cr (‰)
Basal Pongola paleosol	3.0	0.63	−0.13	−0.09
Nsuze paleosol	2.96	1.24	−2.45	−0.26
Saganaga paleosol	2.685	0.51	0.47	0.03
Cooper Lake paleosol	2.45	−0.31	0.20	−0.20
Lauzon Bay paleosol	2.45	−1.94	1.50	−0.17
Pike Lake Road (MCR) paleosol	1.1	0.02	0.10	0.20
Two Harbors (MCR) paleosol	1.1	−0.04	0.00	0.01
Verde River paleosol	0.54	0.08	−0.18	−0.22
St. Francois Mountains paleosol	0.5	−0.79	0.73	−0.11
Olive Hill Clay paleosol	0.323	−0.42	−0.68	0.16

TABLE 3 Effect of weathering on loss/gain of Cr and δ^{53}Cr signature. The dimensionless mass transfer coefficient $\tau_{i,j}$ is calculated (following Anderson et al., 2002) for Cr assuming immobile Al; positive values indicate gain of Cr relative to the parent. The change in δ^{53}Cr due to weathering is based on the amount of loss/gain and the δ^{53}Cr at each measured depth in the paleosol and then integrated over the thickness of the paleosol; we assume in this case that all elemental mobility is due to weathering. This change is then subtracted from the measured δ^{53}Cr to estimate the original value before Cr gain/loss. Estimates of original values are within or very close to the crustal range, suggesting that the calculations of the degree of loss/gain are approximately accurate

3.2 | Elemental geochemistry and weathering

Major and trace element concentrations and ratios (e.g., Fe and Cr) show a change in elemental mobility starting ca. 0.6 Ga. From 3.0 to 1.1 Ga, most paleosols show overall Fe and Mn loss relative to parent or least weathered material (Table 2), as has also been previously reported (Driese et al., 2011; Mitchell & Sheldon, 2009, 2010, 2016; Sutton & Maynard, 1992, 1993), which is consistent with a broadly reducing surface environment (<1% PAL, c.f. Pinto and Holland (1988)). Cr/Al ratios show either loss of Cr in the upper part of the paleosol (basal Pongola, Nsuze, Lauzon Bay, Cooper Lake) or variable profiles (Saganaga, Two Harbors, and Pike Lake Road). In contrast to investigated Archean and Proterozoic paleosols, Phanerozoic paleosols (Verde River, St. Francois Mountains, Olive Hill Clay) show multiple levels of Fe enrichment or depletion but no net overall Fe loss. Like the δ^{53}Cr profiles in these paleosols, Cr/Al profiles are complex, indicating spatially (and/or temporally) variable redox histories. We note that Al/Ti ratios within each paleosol are relatively consistent, indicating minimal input of allochthonous material (e.g., dust; Maynard, 1992), with the exception of St. Francois Mountains and the middle part of the Olive Hill profile.

To assess the mobility of chromium in paleosols, we utilized the mass balance coefficient

$$\tau_{i,j} = \frac{C_{j,w}C_{i,p}}{C_{j,p}C_{i,w}} - 1, \quad (1)$$

where for elemental concentrations, C the subscripts i and j denote immobile and mobile elements, respectively, and p and w denote the parent rock and the weathering product (Anderson, Dietrich, & Brimhall, 2002; Brimhall & Dietrich, 1987). We calculated $\tau_{i,j}$ for Cr integrated over the depth of each paleosol, assuming immobile Al and invariant bulk density (Table 3). This dimensionless coefficient indicates gain or loss of material, and the relative magnitude of that change. Positive and negative values indicate gain and loss of an element, respectively, with τ = 1.0 indicating 100% gain. We also performed a simple mass balance to estimate the effect of gain or loss on the original bulk δ^{53}Cr value (Table 3). The paleosols that show significant net addition of Cr are the Pongola, Nsuze, and Saganaga paleosols, with the former two shifting toward lower δ^{53}Cr and the latter toward higher δ^{53}Cr. Cooper Lake and Lauzon Bay display evidence of significant net loss of Cr, while other Precambrian paleosols (including Two Harbors and Pike Lake Road) exhibit only small net changes (<10%) in total profile Cr content. St. Francois Mountains and Olive Hill Clay also show evidence net loss of Cr, while Verde River shows net gain, but all three show large variation between positive and negative $\tau_{i,j}$ at different depths within the paleosol. This pattern indicates a complex pattern of Cr mobility in space and time (e.g., due to variations in redox conditions and/or mechanical transport), as is common in modern soils. As highlighted above, variations in the δ^{53}Cr of Phanerozoic paleosols are also consistent with this modern-like redox behavior.

4 | DISCUSSION

Our Cr isotope data suggest there was a significant shift in Cr cycling sometime in the Neoproterozoic or earliest Phanerozoic. Archean and mid-Proterozoic Cr isotope data have χ^2 < 1 (Table S1), suggesting that Cr cycling did not experience a long-term secular change at the GOE despite the shift to an oxygenated atmosphere (Farquhar et al., 2000; Konhauser et al., 2011; Lyons et al., 2014). However, the paleosol record provides only a series of snapshots in time from the Archean and Proterozoic and would thus not capture possible excursions in pO_2 (e.g., Gilleaudeau et al., 2016; Zhang et al., 2016). The patterns observed in Archean and Proterozoic paleosol Cr isotope data are distinct from Phanerozoic and modern paleosol data. Unlike Archean and mid-Proterozoic paleosols, Phanerozoic paleosols

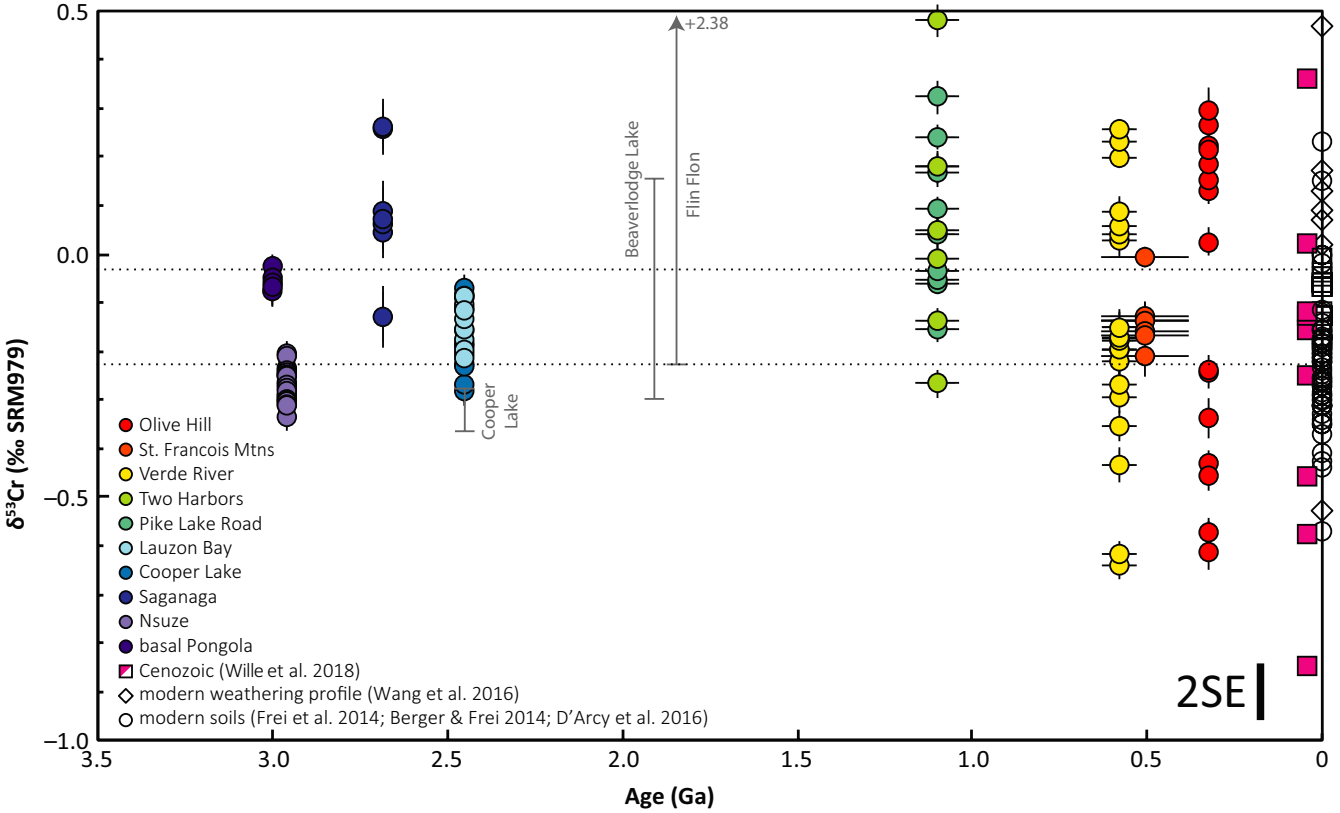

FIGURE 2 Record of chromium isotopes (δ^{53}Cr) in permil (‰ SRM979) in paleosols from 3.0 Ga to present. Error bars on data points indicate uncertainty in age and δ^{53}Cr 2SE. Where error bars do not appear, uncertainty is smaller than symbol size. The range of paleosol δ^{53}Cr data from several Paleoproterozoic paleosols are also plotted as gray bars: 2.45 Ga Cooper Lake (Babechuk et al., 2019), 1.9 Ga Beaverlodge Lake (Toma et al., 2019), and 1.85 Ga Flin Flon (Babechuk et al., 2017). We omit the Schreiber Beach paleosol (Frei & Polat, 2013) owing to the evidence for trace and radiogenic element mobility (see discussion within that paper) and questions about its geologic context (i.e., whether it is a typical paleosol; Fralick et al., 2017). Horizontal dashed lines indicate the crustal (BSE) δ^{53}Cr array (Schoenberg et al., 2008; Wang et al., 2016)

contain clearly sub-crustal δ^{53}Cr values that are an unambiguous signal for net loss of supra-crustal δ^{53}Cr. The 2.96 Ga Nsuze paleosol shows slightly sub-crustal δ^{53}Cr values, but the profile is marked by Cr addition (Table 3) and these values deviate only slightly from the crustal range when mass balance is considered. This paleosol may also have experienced later Cr addition (Albut et al., 2018; Crowe et al., 2013). Given these observations, it is difficult to link the Nsuze δ^{53}Cr data to significant oxidative Cr(VI) loss in a straightforward way.

4.1 | Cr mass transport

The net Cr addition in the Nsuze paleosol highlights the importance of considering Cr mass transport in tandem with isotopic composition (e.g., Konhauser et al., 2011). Figure 4 shows an interpretive framework based on these two axes. Modern soils are dominated by the movement of material with supra-crustal δ^{53}Cr, which is currently viewed as the product of oxidative weathering and ligand complexation (Figure 4a). Paleosol samples from 3.0 to 1.1 Ga largely fall within or close to crustal values, with some 1.1 Ga samples showing supra-crustal δ^{53}Cr (Figure 4b). In the Phanerozoic, the range of samples closely resembles modern behavior, although loss of Cr appears more common than gain in these paleosols (Table 3). As outlined above, the classic Cr isotope framework (Frei et al., 2009) posits that loss of ^{53}Cr-enriched matter from a paleosol as Cr(VI), as is observed in modern soils (e.g., Berger & Frei, 2014; Frei et al., 2014; Wang et al., 2016; Wille et al., 2018), is the most obvious signal for a well-oxygenated weathering environment. The additional consideration of transport agrees with that, but also explains potential variation beyond the classic framework due to gain or loss of Cr in paleosols. Taken as a whole, our record suggests the onset of a fully oxidative Cr cycle in the terrestrial environment—based on our snapshots through Earth's history—occurred sometime between ~1.1 and ~0.6 Ga.

The observed Cr isotope variability in the >0.6 Ga paleosols is most likely tied to small-scale Cr oxidation, given the absence of modern-like Cr cycling in soils and the lack of other kinds of evidence for long-term, globally extensive oxidative weathering. In the traditional stable Cr isotope framework, δ^{53}Cr variations beyond the observed igneous range are linked to Cr redox cycling (Frei et al., 2009). The recognition that Cr could have been oxidized and then re-reduced elsewhere in the terrestrial environment, as has been emphasized

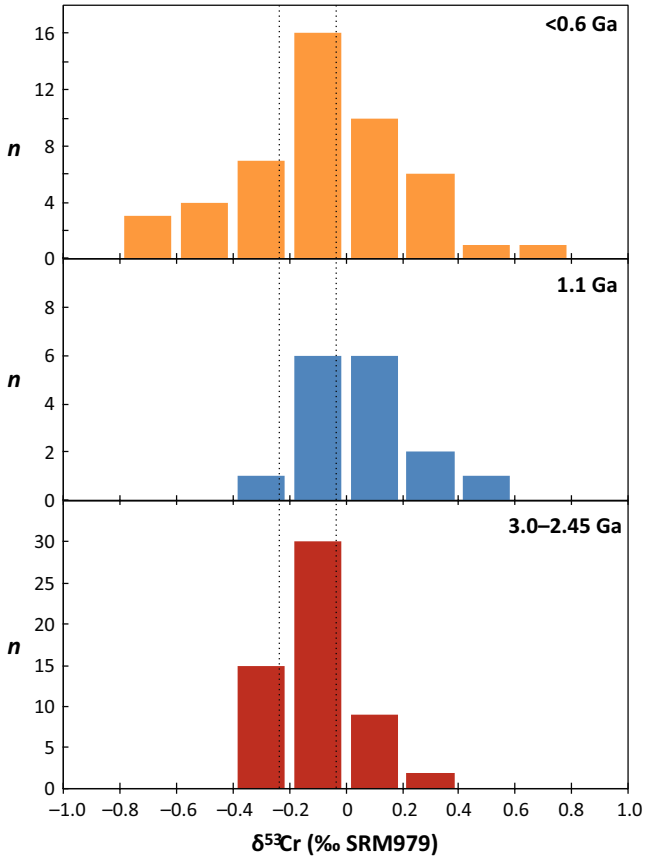

FIGURE 3 Histograms of chromium isotope values (δ^{53}Cr) in permil (‰ SRM979) of paleosols in three-time slices. From 3.0 to 1.1 Ga, paleosols show largely crustal or above crustal values; by ca. 0.6 Ga, paleosols show a modern range of values reflecting both oxidation and reduction of Cr at different levels within the soil. Dashed lines indicate the crustal (BSE) array (Schoenberg et al., 2008; Wang et al., 2016). The Flin Flon paleosol data are omitted from the second time slice, as the values are anomalous and there are multiple explanations for them independent of atmospheric redox state (see discussion in Babechuk et al., 2017)

by D'Arcy et al. (2016), indicates that the traditional framework for interpreting stable Cr data must be extended. Simple kinetic modeling indicates that Cr oxidation can proceed at pO_2 < 0.1% PAL (Planavsky et al., 2014), which is below estimates for the amount of oxygen needed to quantitatively oxidize iron within the weathering realm (pO_2 > 1% PAL; e.g., Crowe et al., 2013; Holland & Zbinden, 1988; Pinto & Holland, 1988). As long as a significant reductant load (e.g., Fe^{2+}) is present in soils, it would result in the (quantitative) re-reduction of any Cr that was oxidized. Therefore, it is possible that Cr would be oxidized in the uppermost portion of the soil horizon by atmospheric O_2, then re-reduced and quantitatively trapped onto iron oxides or ferruginous clays in a lower portion of the soil profile (e.g., Frei & Polat, 2013). Such a history of repeated oxidation and reduction is strongly suggested by the presence of supra-crustal δ^{53}Cr values in paleosols as early as 2.685 Ga (Figure 2) and is consistent with the addition of Cr to some soil profiles (Table 3). This framework reconciles the observed loss of Fe from the Archean and Proterozoic weathering profiles with evidence for Cr oxidation and indicates atmospheric oxygen levels <1% PAL through the Precambrian.

4.2 | Ligands

Alternatively, the observed Cr isotope variability within Archean and Proterozoic paleosols could be tied to Cr(III)-organic complexation instead of local Cr redox cycling. Although there was certainly a shift in the extent of terrestrialization with the rise of land plants in the Paleozoic (e.g., Berner, 1992; Kenrick, Wellman, Schneider, & Edgecombe, 2012), there is likely to have been a terrestrial biosphere as early as the Archean (e.g., Rye & Holland, 2000; Stüeken, Catling, & Buick, 2012; Watanabe, Martini, & Ohmoto, 2000). It is thus important to consider biotic weathering effects, even in Precambrian paleosols (Driese et al., 2011). Complexation between ligands and Cr could potentially produce either ^{53}Cr-enriched or ^{53}Cr-depleted mobile Cr, making it difficult to pinpoint the effects of such complexation (Babechuk et al., 2018; Saad et al., 2017). Although there are no obvious indicators of extensive biotic weathering in our pre-Carboniferous paleosols (e.g., they are not organic-rich, they lack root traces or burrows), some degree of biotic mediation of the weathering is still possible. For instance, Driese et al. (2011) used elemental (Fe, P, Cu, Y) and mineralogical data from the Saganaga paleosol (which shows supra-crustal δ^{53}Cr values) to suggest extensive ligand complexation during soil formation. Furthermore, we cannot rule out the possibility that the wide range and non-crustal δ^{53}Cr values seen in modern and Phanerozoic paleosols may be partially due to organic complexation. This is one possible explanation for the extreme supra-crustal δ^{53}Cr values reported in the ca. 1.85 Ga Flin Flon paleosol (Figure 2; Babechuk et al., 2017). We emphasize that, while it is impossible to tell whether an individual Cr isotope value is due to oxidative weathering processes or ligand complexation, the presence of ligands does not explain the appearance of significant loss of isotopically heavy Cr in the late Proterozoic–Cambrian.

4.3 | Small-scale terrestrial oxidative weathering

Terrestrial biotic communities may have also affected the local redox state of the studied paleosols. Terrestrial cyanobacterial mats can have very high rates of oxygen production, and peak oxygen concentrations are essentially decoupled from overlying atmospheric oxygen levels (e.g., Lalonde & Konhauser, 2015; Zhao, Reinhard, & Planavsky, 2017). Therefore, oxidation could potentially occur in the uppermost portion of a soil profile because of localized oxygen production rather than coupling with a high-pO_2 atmosphere. Conversely, a terrestrial community could increase the reductant load within a soil profile, potentially changing the minimum oxygen concentrations that are needed to quantitatively oxidize and retain Fe or to mobilize Cr and thus isotopically fractionate it (e.g., Crowe et al., 2013; Lenton & Daines, 2017b). However, given that active organic production would likely be restricted to the high porosity, continually-eroding portion of a soil profile, we consider it unlikely that cyanobacterial mats

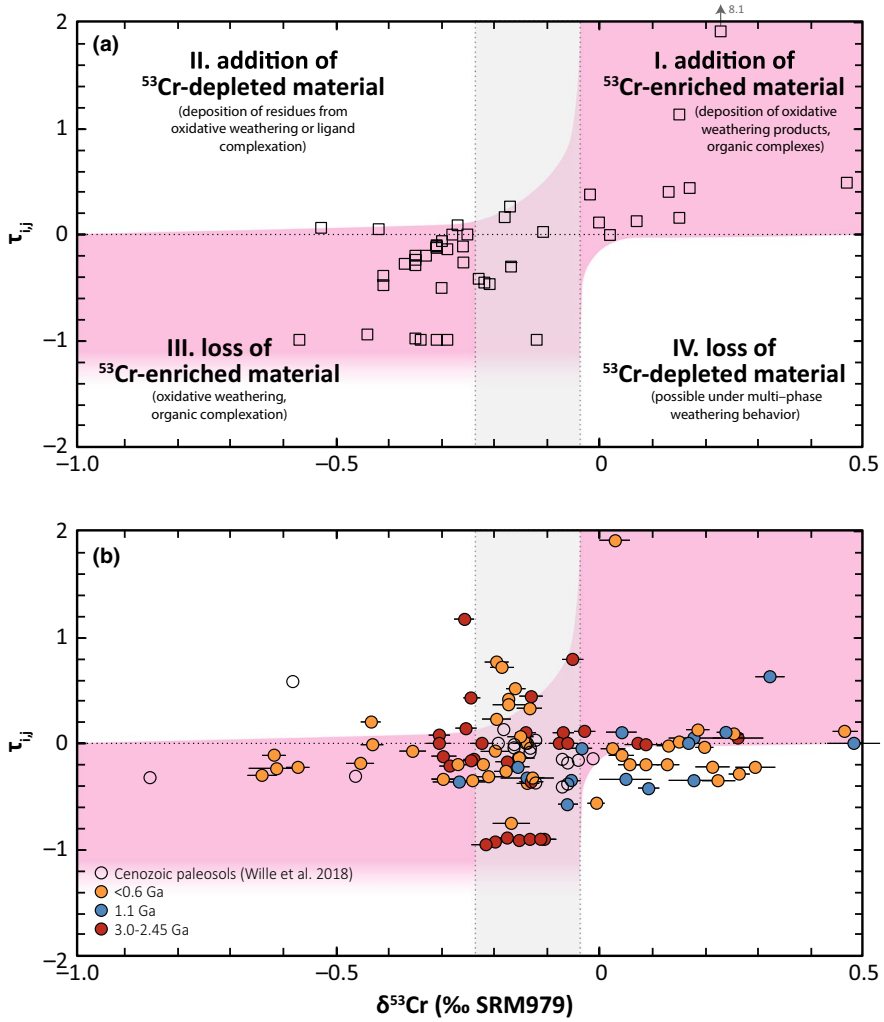

FIGURE 4 Framework for interpreting Cr isotope values in paleosols. Combining the δ^{53}Cr signature with an expression of the gain/loss of Cr from the soil better expresses the complexity of Cr mobility. The crustal (BSE) δ^{53}Cr array (Schoenberg et al., 2008; Wang et al., 2016) is shown in gray. Modern soil δ^{53}Cr (panel a, from Berger & Frei, 2014; D'Arcy et al., 2016; Frei et al., 2014; Wang et al., 2016) reflects movement of material with supra-crustal δ^{53}Cr (quadrants I and III). Paleosol samples (b) are largely confined to crustal values from 3.01.1 Ga. From 0.6 Ga to present, the range of samples more closely resembles modern behavior, with loss of Cr appears more common than gain. Essentially no modern samples and few paleosol samples plot in quadrants II and IV, which result from the mobilization of weathering residues with sub-crustal δ^{53}Cr. Such behavior is possible, but is uncommon in modern soils, which are dominated by oxidative weathering and organic activity

would dramatically increase the amount of oxygen that diffuses into a total soil profile. This conclusion is supported by the sediments of the 1.1 Ga North Shore Volcanic Group (containing the Mid-Continent Rift paleosols), which contain both microbial mats (Elmore, 1983, 1984; Sheldon, 2012) and paleosols that indicate relatively low pO_2. Waterlogged or wetland soils would be likely to develop thicker cyanobacterial mats (see discussion in Zhao et al., 2017) and thus could have represented an exception to this rule, although they also might have accumulated more reductants. While unlikely, it nevertheless remains a possibility that terrestrial microbial communities could potentially have induced Cr oxidation independent of atmospheric redox state, thus complicating the interpretation of observed Cr isotope variability.

4.4 | Paleosol records in context

Relative to marine records (e.g., iron formations, black shales, carbonates), our paleosol record has the distinct advantage that it formed in direct contact with the atmosphere. Our long-term record brackets the secular change from minor to widespread Cr oxidation in the Neoproterozoic; however, paleosols lack the temporal coverage and continuity achievable by marine records. Marine shales (Cole et al., 2016) and iron formations (Planavsky et al., 2014) provide evidence for the onset of oxidative Cr cycling at ~800 Ma, which is compatible with our record (however, c.f. Canfield et al., 2018). Although all signals for early oxygenation should be vetted for effects of later alteration (see Albut et al., 2018), there are intervals earlier in the Proterozoic that show strongly fractionated Cr isotope values, which are consistent with transient intervals of oxygenation (Canfield et al., 2018; Diamond & Lyons, 2018; Fralick et al., 2017; Frei et al., 2009; Gilleaudeau et al., 2016; Zhang et al., 2016). A vague picture of the temporally and/or spatially confined nature of these pulses may be drawn from a cluster of ca. 1.9–1.8 Ga paleosols and marine sediments from Canada, which show quite different ranges of δ^{53}Cr (Figure 2), as well as variable Fe mobility (Babechuk et al., 2017; Bellefroid et al., 2018; Frei & Polat, 2013; Toma, Holmden, Shakotko, Pan, & Ootes, 2019). The redox conditions that prevailed in any one of these paleosols appear to have been localized in time and/or space, as the majority of Proterozoic paleosols as well as marine records indicate that the background state was one of limited (<1% PAL) atmospheric oxygen. This study highlights the importance of transport and Cr isotope fractionation processes in paleosols beyond oxidative weathering. We look forward to future studies that

carefully interrogate both redox-related and non-redox-related mechanisms and their importance in Earth's ancient and modern Cr cycle.

5 | CONCLUSIONS

Our composite record of paleosol geochemistry provides a series of snapshots into evolution of surface oxygen levels from 3.0 Ga into the Phanerozoic. These data add to a growing body of work suggesting a widespread, permanent, stepwise increase in baseline atmospheric pO_2 to >1% PAL during the Neoproterozoic. Given that we only have snapshots from Earth's history, our record does not clash with the idea of brief intervals of high oxygen during the Precambrian. The paleosols also provide potential, though not definitive, evidence for the occurrence of some degree of localized oxidative Cr cycling since at least 2.685 Ga. Future work on Meso- and Neoproterozoic paleosols will help to more tightly constrain the nature and timing of the expansion of atmospheric O_2 levels above those required for the production and maintenance of a large ^{53}Cr-enriched Cr(VI) reservoir at Earth's surface, as well as offering valuable insights into linkages and lags between the oxygenation of the atmosphere and deep ocean and a potentially dynamic Earth surface O_2 cycle during Proterozoic time.

ACKNOWLEDGMENTS

This work was improved by discussions with Sean Crowe, Kurt Konhauser, and Lou Derry. We appreciate assistance with information about selected paleosols from Sally Sutton and laboratory assistance from Brian DeCorte. Support for this work was provided by the NASA Astrobiology Institute and the NSF Earth-Life Transitions program to NJP and CTR, and NSF EAR-1050760 to NDS.

CONFLICT OF INTEREST

The authors declare no conflicts of interest or competing financial interests.

ORCID

David Auerbach Colwyn https://orcid.org/0000-0002-9675-3925

Nathan D. Sheldon https://orcid.org/0000-0003-3371-0036

REFERENCES

Albut, G., Babechuk, M. G., Kleinhanns, I. C., Benger, M., Beukes, N. J., Steinhilber, B., … Schoenberg, R. (2018). Modern rather than Mesoarchaean oxidative weathering responsible for the heavy stable Cr isotopic signatures of the 2.95 Ga old Ijzermijn iron formation (South Africa). *Geochimica et Cosmochimica Acta*, *228*, 157–189.

Anbar, A. D., Duan, Y., Lyons, T. W., Arnold, G. L., Kendall, B., Creaser, R. A., … Garvin, J. (2007). A whiff of oxygen before the Great Oxidation Event? *Science*, *317*(5846), 1903–1906.

Anderson, S. P., Dietrich, W. E., & Brimhall, G. H. (2002). Weathering profiles, mass-balance analysis, and rates of solute loss: Linkages between weathering and erosion in a small, steep catchment. *Geological Society of America Bulletin*, *114*(9), 1143–1158.

Babechuk, M. G., Kleinhanns, I. C., Reitter, E., & Schoenberg, R. (2018). Kinetic stable Cr isotopic fractionation between aqueous Cr (III)-Cl-H2O complexes at 25° C: Implications for Cr (III) mobility and isotopic variations in modern and ancient natural systems. *Geochimica et Cosmochimica Acta*, *222*, 383–405.

Babechuk, M. G., Kleinhanns, I. C., & Schoenberg, R. (2017). Chromium geochemistry of the ca. 1.85 Ga Flin Flon paleosol. *Geobiology*, *15*(1), 30–50.

Babechuk, M. G., Weimar, N. E., Kleinhanns, I. C., Eroglu, S., Swanner, E. D., Kenny, G. G., … Schoenberg, R. (2019). Pervasively anoxic surface conditions at the onset of the Great Oxidation Event: New multi-proxy constraints from the Cooper Lake paleosol. *Precambrian Research*, *323*, 126–163. https://doi.org/10.1016/j.precamres.2018.12.029

Bellefroid, E. J., Hood, A. V. S., Hoffman, P. F., Thomas, M. D., Reinhard, C. T., & Planavsky, N. J. (2018). Constraints on Paleoproterozoic atmospheric oxygen levels. *Proceedings of the National Academy of Sciences of the United States of America*, *115*(32), 8104–8109. https://doi.org/10.1073/pnas.1806216115

Berger, A., & Frei, R. (2014). The fate of chromium during tropical weathering: A laterite profile from Central Madagascar. *Geoderma*, *213*, 521–532. https://doi.org/10.1016/j.geoderma.2013.09.004

Berner, R. A. (1992). Weathering, plants, and the long-term carbon cycle. *Geochimica et Cosmochimica Acta*, *56*(8), 3225–3231. https://doi.org/10.1016/0016-7037(92)90300-8

Brimhall, G. H., & Dietrich, W. E. (1987). Constitutive mass balance relations between chemical composition, volume, density, porosity, and strain in metasomatic hydrochemical systems: Results on weathering and pedogenesis. *Geochimica et Cosmochimica Acta*, *51*(3), 567–587. https://doi.org/10.1016/0016-7037(87)90070-6

Canfield, D. E. (1998). A new model for Proterozoic ocean chemistry. *Nature*, *396*(6710), 450–453.

Canfield, D. E. (2005). The early history of atmospheric oxygen: Homage to Robert M. Garrels. *Annual Review of Earth and Planetary Sciences*, *33*, 1–36. https://doi.org/10.1146/annurev.earth.33.092203.122711

Canfield, D. E., Poulton, S. W., & Narbonne, G. M. (2007). Late-Neoproterozoic deep-ocean oxygenation and the rise of animal life. *Science*, *315*(5808), 92–95.

Canfield, D. E., Zhang, S., Frank, A. B., Wang, X., Wang, H., Su, J., … Frei, R. (2018). Highly fractionated chromium isotopes in Mesoproterozoic-aged shales and atmospheric oxygen. *Nature Communications*, *9*(1), 2871. https://doi.org/10.1038/s41467-018-05263-9

Cole, D. B., O'Connell, B., & Planavsky, N. J. (2018). Authigenic chromium enrichments in Proterozoic ironstones. *Sedimentary Geology*, *372*, 25–43. https://doi.org/10.1016/j.sedgeo.2018.05.002

Cole, D. B., Reinhard, C. T., Wang, X., Gueguen, B., Halverson, G. P., Gibson, T., … Planavsky, N. J. (2016). A shale-hosted Cr isotope record of low atmospheric oxygen during the Proterozoic. *Geology*, *44*(7), 555–558. https://doi.org/10.1130/G37787.1

Crockford, P. W., Hayles, J. A., Bao, H., Planavsky, N. J., Bekker, A., Fralick, P. W., … Wing, B. A. (2018). Triple oxygen isotope evidence for limited mid-Proterozoic primary productivity. *Nature*, *559*(7715), 613. https://doi.org/10.1038/s41586-018-0349-y

Crowe, S. A., Døssing, L. N., Beukes, N. J., Bau, M., Kruger, S. J., Frei, R., & Canfield, D. E. (2013). Atmospheric oxygenation three billion years ago. *Nature*, *501*(7468), 535–538.

Daines, S. J., Mills, B. J., & Lenton, T. M. (2017). Atmospheric oxygen regulation at low Proterozoic levels by incomplete oxidative weathering of sedimentary organic carbon. *Nature Communications*, *8*, 14379. https://doi.org/10.1038/ncomms14379

Dann, J. C., Chamberlain, K., & Bowring, S. (1989). *An Early Proterozoic ophiolite, central Arizona: UPb constraints on its structure and development*. Paper presented at the Geological Society of America Abstracts with Programs.

D'Arcy, J., Babechuk, M. G., Døssing, L. N., Gaucher, C., & Frei, R. (2016). Processes controlling the chromium isotopic composition of river water: Constraints from basaltic river catchments. *Geochimica et Cosmochimica Acta*, *186*, 296–315. https://doi.org/10.1016/j.gca.2016.04.027

DeCelles, P. G., Carrapa, B., Horton, B., & Gehrels, G. E. (2011). Cenozoic foreland basin system in the central Andes of northwestern Argentina: Implications for Andean geodynamics and modes of deformation. *Tectonics*, *30*(6). https://doi.org/10.1029/2011TC002948

Delvigne, C., Opfergelt, S., Cardinal, D., Hofmann, A., & André, L. (2016). Desilication in Archean weathering processes traced by silicon isotopes and Ge/Si ratios. *Chemical Geology*, *420*, 139–147.

Diamond, C. W., & Lyons, T. W. (2018). Mid-Proterozoic redox evolution and the possibility of transient oxygenation events. *Emerging Topics in Life Sciences*, *2*, 235–245. https://doi.org/10.1042/ETLS20170146

Driese, S. G., Jirsa, M. A., Ren, M., Brantley, S. L., Sheldon, N. D., Parker, D., & Schmitz, M. (2011). Neoarchean paleoweathering of tonalite and metabasalt: Implications for reconstructions of 2.69 Ga early terrestrial ecosystems and paleoatmospheric chemistry. *Precambrian Research*, *189*(1), 1–17.

Ellis, A. S., Johnson, T. M., & Bullen, T. D. (2002). Chromium isotopes and the fate of hexavalent chromium in the environment. *Science*, *295*(5562), 2060–2062.

Elmore, R. D. (1983). Precambrian non-marine stromatolites in alluvial fan deposits, the Copper Harbor Conglomerate, upper Michigan. *Sedimentology*, *30*(6), 829–842. https://doi.org/10.1111/j.1365-3091.1983.tb00713.x

Elmore, R. D. (1984). The Copper Harbor Conglomerate: A late Precambrian fining-upward alluvial fan sequence in northern Michigan. *Geological Society of America Bulletin*, *95*(5), 610–617. https://doi.org/10.1130/0016-7606(1984)95<610:TCHCAL>2.0.CO;2

Erwin, D. H., Laflamme, M., Tweedt, S. M., Sperling, E. A., Pisani, D., & Peterson, K. J. (2011). The Cambrian conundrum: Early divergence and later ecological success in the early history of animals. *Science*, *334*(6059), 1091–1097.

Farquhar, J., Bao, H., & Thiemens, M. (2000). Atmospheric influence of Earth's earliest sulfur cycle. *Science*, *289*(5480), 756–758.

Farquhar, J., Zerkle, A. L., & Bekker, A. (2011). Geological constraints on the origin of oxygenic photosynthesis. *Photosynthesis Research*, *107*(1), 11–36. https://doi.org/10.1007/s11120-010-9594-0

Fralick, P., Planavsky, N., Burton, J., Jarvis, I., Addison, W., Barrett, T., & Brumpton, G. (2017). Geochemistry of Paleoproterozoic Gunflint Formation carbonate: Implications for hydrosphere-atmosphere evolution. *Precambrian Research*, *290*, 126–146. https://doi.org/10.1016/j.precamres.2016.12.014

Frei, R., Gaucher, C., Poulton, S. W., & Canfield, D. E. (2009). Fluctuations in Precambrian atmospheric oxygenation recorded by chromium isotopes. *Nature*, *461*(7261), 250–253.

Frei, R., Poiré, D., & Frei, K. M. (2014). Weathering on land and transport of chromium to the ocean in a subtropical region (Misiones, NW Argentina): A chromium stable isotope perspective. *Chemical Geology*, *381*, 110–124. https://doi.org/10.1016/j.chemgeo.2014.05.015

Frei, R., & Polat, A. (2013). Chromium isotope fractionation during oxidative weathering—Implications from the study of a Paleoproterozoic (ca. 1.9 Ga) paleosol, Schreiber Beach, Ontario, Canada. *Precambrian Research*, *224*, 434–453. https://doi.org/10.1016/j.precamres.2012.10.008

Gilleaudeau, G. J., Frei, R., Kaufman, A. J., Kah, L. C., Azmy, K., Bartley, J. K., … Knoll, A. H. (2016). Oxygenation of the mid-Proterozoic atmosphere: Clues from chromium isotopes in carbonates. *Geochemical Perspectives Letters*, *2*, 178–187. https://doi.org/10.7185/geochemlet.1618

Goldblatt, C., Lenton, T. M., & Watson, A. J. (2006). Bistability of atmospheric oxygen and the Great Oxidation. *Nature*, *443*(7112), 683–686.

Grandstaff, D., Edelman, M., Foster, R., Zbinden, E., & Kimberley, M. (1986). Chemistry and mineralogy of Precambrian paleosols at the base of the Dominion and Pongola Groups (Transvaal, South Africa). *Precambrian Research*, *32*(2), 97–131.

Green, J. C., & Fitz, T. J. III (1993). Extensive felsic lavas and rheoignimbrites in the Keweenawan Midcontinent Rift plateau volcanics, Minnesota: Petrographic and field recognition. *Journal of Volcanology and Geothermal Research*, *54*(3–4), 177–196.

Gueguen, B., Reinhard, C. T., Algeo, T. J., Peterson, L. C., Nielsen, S. G., Wang, X., … Planavsky, N. J. (2016). The chromium isotope composition of reducing and oxic marine sediments. *Geochimica et Cosmochimica Acta*, *184*, 1–19. https://doi.org/10.1016/j.gca.2016.04.004

Halevy, I., Johnston, D. T., & Schrag, D. P. (2010). Explaining the structure of the Archean mass-independent sulfur isotope record. *Science*, *329*(5988), 204–207.

Hardisty, D. S., Lu, Z., Bekker, A., Diamond, C. W., Gill, B. C., Jiang, G., … Lyons, T. W. (2017). Perspectives on Proterozoic surface ocean redox from iodine contents in ancient and recent carbonate. *Earth and Planetary Science Letters*, *463*, 159–170. https://doi.org/10.1016/j.epsl.2017.01.032

Holland, H. D. (2006). The oxygenation of the atmosphere and oceans. *Philosophical Transactions of the Royal Society B: Biological Sciences*, *361*(1470), 903–915.

Holland, H. D., & Zbinden, E. A. (1988). Paleosols and the evolution of the atmosphere: Part I. In A. Lerman & M. Meybeck (Eds.), *Physical and chemical weathering in geochemical cycles* (pp. 61–82). Dordrecht, The Netherlands: Springer.

Jenny, H. (1941). *Factors of soil formation*. New York, NY: McGraw-Hill Book Company.

Kendall, B., Brennecka, G. A., Weyer, S., & Anbar, A. D. (2013). Uranium isotope fractionation suggests oxidative uranium mobilization at 2.50 Ga. *Chemical Geology*, *362*, 105–114. https://doi.org/10.1016/j.chemgeo.2013.08.010

Kenrick, P., Wellman, C. H., Schneider, H., & Edgecombe, G. D. (2012). A timeline for terrestrialization: Consequences for the carbon cycle in the Palaeozoic. *Philosophical Transactions of the Royal Society B: Biological Sciences*, *367*(1588), 519–536.

Ketchum, K. Y., Heaman, L. M., Bennett, G., & Hughes, D. J. (2013). Age, petrogenesis and tectonic setting of the Thessalon volcanic rocks, Huronian Supergroup, Canada. *Precambrian Research*, *233*, 144–172.

Kimberley, M. M., & Grandstaff, D. E. (1986). Profiles of elemental concentrations in Precambrian paleosols on basaltic and granitic parent materials. *Precambrian Research*, *32*(2–3), 133–154.

Knoll, A. H., Bergmann, K. D., & Strauss, J. V. (2016). Life: The first two billion years. *Philosophical Transactions of the Royal Society B: Biological Sciences*, *371*(1707), 20150493. https://doi.org/10.1098/rstb.2015.0493

Knoll, A. H., & Sperling, E. A. (2014). Oxygen and animals in Earth history. *Proceedings of the National Academy of Sciences of the United States of America*, *111*(11), 3907–3908. https://doi.org/10.1073/pnas.1401745111

Konhauser, K. O., Lalonde, S. V., Planavsky, N. J., Pecoits, E., Lyons, T. W., Mojzsis, S. J., … Bekker, A. (2011). Aerobic bacterial pyrite oxidation and acid rock drainage during the Great Oxidation Event. *Nature*, *478*(7369), 369–373. https://doi.org/10.1038/nature10511

Krogh, T., Davis, D., & Corfu, F. (1984). Precise U-Pb zircon and baddeleyite ages for the Sudbury area. In E. G. Pye, A. J. Naldrett, & P. E. Giblin

(Eds.), *The geology and ore deposits of the Sudbury structure* (Vol. *1*, pp. 431–446). Sudbury, Canada: Ontario Geological Survey.

Kump, L. R. (2008). The rise of atmospheric oxygen. *Nature*, *451*(7176), 277–278.

Lalonde, S. V., & Konhauser, K. O. (2015). Benthic perspective on Earth's oldest evidence for oxygenic photosynthesis. *Proceedings of the National Academy of Sciences of the United States of America*, *112*(4), 995–1000. https://doi.org/10.1073/pnas.1415718112

Lenton, T. M., & Daines, S. J. (2017a). Biogeochemical transformations in the history of the ocean. *Annual Review of Marine Science*, *9*, 31–58. https://doi.org/10.1146/annurev-marine-010816-060521

Lenton, T. M., & Daines, S. J. (2017b). Matworld-The biogeochemical effects of early life on land. *New Phytologist*, *215*(2), 531–537. https://doi.org/10.1111/nph.14338

Lenton, T. M., Daines, S. J., & Mills, B. J. (2018). COPSE reloaded: An improved model of biogeochemical cycling over Phanerozoic time. *Earth-Science Reviews*, *178*, 1–28. https://doi.org/10.1016/j.earscirev.2017.12.004

Li, C., Planavsky, N. J., Love, G. D., Reinhard, C. T., Hardisty, D., Feng, L., … Lyons, T. W. (2015). Marine redox conditions in the middle Proterozoic ocean and isotopic constraints on authigenic carbonate formation: Insights from the Chuanlinggou Formation, Yanshan Basin, North China. *Geochimica et Cosmochimica Acta*, *150*, 90–105. https://doi.org/10.1016/j.gca.2014.12.005

Lyons, T. W., Fike, D. A., & Zerkle, A. (2015). Emerging biogeochemical views of Earth's ancient microbial worlds. *Elements*, *11*(6), 415–421. https://doi.org/10.2113/gselements.11.6.415

Lyons, T. W., Reinhard, C. T., & Planavsky, N. J. (2014). The rise of oxygen in Earth's early ocean and atmosphere. *Nature*, *506*(7488), 307–315.

Maynard, J. (1992). Chemistry of modern soils as a guide to interpreting Precambrian paleosols. *The Journal of Geology*, *00*, 279–289. https://doi.org/10.1086/629632

Mitchell, R. L., & Sheldon, N. D. (2009). Weathering and paleosol formation in the 1.1 Ga Keweenawan Rift. *Precambrian Research*, *168*(3), 271–283. https://doi.org/10.1016/j.precamres.2008.09.013

Mitchell, R. L., & Sheldon, N. D. (2010). The ~1100 Ma Sturgeon Falls paleosol revisited: Implications for Mesoproterozoic weathering environments and atmospheric CO2 levels. *Precambrian Research*, *183*(4), 738–748. https://doi.org/10.1016/j.precamres.2010.09.003

Mitchell, R. L., & Sheldon, N. D. (2016). Sedimentary provenance and weathering processes in the 1.1 Ga Midcontinental Rift of the Keweenaw Peninsula, Michigan, USA. *Precambrian Research*, *275*, 225–240. https://doi.org/10.1016/j.precamres.2016.01.017

Mukasa, S. B., Wilson, A. H., & Young, K. R. (2013). Geochronological constraints on the magmatic and tectonic development of the Pongola Supergroup (Central Region), South Africa. *Precambrian Research*, *224*, 268–286.

Murakami, T., Matsuura, K., & Kanzaki, Y. (2016). Behaviors of trace elements in Neoarchean and Paleoproterozoic paleosols: Implications for atmospheric oxygen evolution and continental oxidative weathering. *Geochimica et Cosmochimica Acta*, *192*, 203–219. https://doi.org/10.1016/j.gca.2016.07.008

Och, L. M., & Shields-Zhou, G. A. (2012). The Neoproterozoic oxygenation event: Environmental perturbations and biogeochemical cycling. *Earth-Science Reviews*, *110*(1), 26–57. https://doi.org/10.1016/j.earscirev.2011.09.004

Ojakangas, R. W., Morey, G. B., & Green, J. C. (2001). The Mesoproterozoic midcontinent rift system, Lake Superior region, USA. *Sedimentary Geology*, *141*, 421–442.

Partin, C., Lalonde, S. V., Planavsky, N., Bekker, A., Rouxel, O., Lyons, T., & Konhauser, K. (2013). Uranium in iron formations and the rise of atmospheric oxygen. *Chemical Geology*, *362*, 82–90. https://doi.org/10.1016/j.chemgeo.2013.09.005

Pavlov, A., & Kasting, J. (2002). Mass-independent fractionation of sulfur isotopes in Archean sediments: Strong evidence for an anoxic Archean atmosphere. *Astrobiology*, *2*(1), 27–41. https://doi.org/10.1089/153110702753621321

Pinto, J. P., & Holland, H. D. (1988). Paleosols and the evolution of the atmosphere, Part II. *Geological Society of America Special Paper*, *216*, 21–34.

Planavsky, N. J., Cole, D. B., Isson, T. T., Reinhard, C. T., Crockford, P. W., Sheldon, N. D., & Lyons, T. W. (2018). A case for low atmospheric oxygen levels during Earth's middle history. *Emerging Topics in Life Sciences*, *2*(2), 149–159. https://doi.org/10.1042/ETLS20170161

Planavsky, N. J., Cole, D. B., Reinhard, C. T., Diamond, C., Love, G. D., Luo, G., … Lyons, T. W. (2016). No evidence for high atmospheric oxygen levels 1,400 million years ago. *Proceedings of the National Academy of Sciences of the United States of America*, *113*(19), E2550–E2551. https://doi.org/10.1073/pnas.1601925113

Prasad, N., & Roscoe, S. M. (1991). Profiles of altered zones at ca. 2.45 Ga unconformities beneath Huronian strata, Elliot Lake, Ontario; evidence for early Aphebian weathering under anoxic conditions. *Geological Survey of Canada*, *Paper C*, *91*, 43–54.

Planavsky, N. J., Reinhard, C. T., Wang, X., Thomson, D., McGoldrick, P., Rainbird, R. H., … Lyons, T. W. (2014). Low Mid-Proterozoic atmospheric oxygen levels and the delayed rise of animals. *Science*, *346*(6209), 635–638.

Rasmussen, B., Bekker, A., & Fletcher, I. R. (2013). Correlation of Paleoproterozoic glaciations based on U–Pb zircon ages for tuff beds in the Transvaal and Huronian Supergroups. *Earth and Planetary Science Letters*, *382*, 173–180.

Reinhard, C. T., Planavsky, N. J., & Lyons, T. W. (2013). Long-term sedimentary recycling of rare sulphur isotope anomalies. *Nature*, *497*(7447), 100–103.

Reinhard, C. T., Planavsky, N. J., Robbins, L. J., Partin, C. A., Gill, B. C., Lalonde, S. V., Lyons, T. W.. (2013). Proterozoic ocean redox and biogeochemical stasis. *Proceedings of the National Academy of Sciences of the United States of America*, *110*(14), 5357–5362. https://doi.org/10.1073/pnas.1208622110

Reinhard, C. T., Planavsky, N. J., Wang, X., Fischer, W. W., Johnson, T. M., & Lyons, T. W. (2014). The isotopic composition of authigenic chromium in anoxic marine sediments: A case study from the Cariaco Basin. *Earth and Planetary Science Letters*, *407*, 9–18. https://doi.org/10.1016/j.epsl.2014.09.024

Robbins, L. J., Lalonde, S. V., Planavsky, N. J., Partin, C. A., Reinhard, C. T., Kendall, B., … Konhauser, K. O. (2016). Trace elements at the intersection of marine biological and geochemical evolution. *Earth-Science Reviews*, *163*, 323–348. https://doi.org/10.1016/j.earscirev.2016.10.013

Rye, R., & Holland, H. D. (1998). Paleosols and the evolution of atmospheric oxygen: A critical review. *American Journal of Science*, *298*(8), 621–672. https://doi.org/10.2475/ajs.298.8.621

Rye, R., & Holland, H. D. (2000). Life associated with a 2.76 Ga ephemeral pond?: Evidence from Mount Roe# 2 paleosol. *Geology*, *28*(6), 483–486.

Saad, E. M., Wang, X., Planavsky, N. J., Reinhard, C. T., & Tang, Y. (2017). Redox-independent chromium isotope fractionation induced by ligand-promoted dissolution. *Nature Communications*, *8*(1), 1590. https://doi.org/10.1038/s41467-017-01694-y

Schoenberg, R., Zink, S., Staubwasser, M., & Von Blanckenburg, F. (2008). The stable Cr isotope inventory of solid Earth reservoirs determined by double spike MC-ICP-MS. *Chemical Geology*, *249*(3), 294–306. https://doi.org/10.1016/j.chemgeo.2008.01.009

Scott, C. T., Bekker, A., Reinhard, C. T., Schnetger, B., Krapež, B., Rumble, D., & Lyons, T. W. (2011). Late Archean euxinic conditions before the rise of atmospheric oxygen. *Geology*, *39*(2), 119–122. https://doi.org/10.1130/G31571.1

Sheldon, N. D. (2006). Precambrian paleosols and atmospheric CO_2 levels. *Precambrian Research*, *147*(1–2), 148–155. https://doi.org/10.1016/j.precamres.2006.02.004

Sheldon, N. D. (2012). Microbially induced sedimentary structures in the ca. 1100 Ma terrestrial midcontinent rift of North America. *Microbial Mats in Siliciclastic Depositional Systems Through Time: SEPM Special Publication 11* (pp. 153–162).

Smyth, A. L., (1984). *Pedogenesis and diagenesis of the Olive Hill Clay Bed, Breathitt Formation (Carboniferous) Northeastern Kentucky*. M.S. thesis, University of Cinncinnati.

Stüeken, E. E., Catling, D. C., & Buick, R. (2012). Contributions to late Archaean sulphur cycling by life on land. *Nature Geoscience*, *5*(10), 722–725. https://doi.org/10.1038/ngeo1585

Sutton, S., & Maynard, J. B. (1992). Multiple alteration events in the history of a sub-Huronian regolith at Lauzon Bay, Ontario. *Canadian Journal of Earth Sciences*, *29*(3), 432–445. https://doi.org/10.1139/e92-038

Sutton, S., & Maynard, J. B. (1993). Sediment-and basalt-hosted regoliths in the Huronian supergroup: Role of parent lithology in middle Precambrian weathering profiles. *Canadian Journal of Earth Sciences*, *30*(1), 60–76. https://doi.org/10.1139/e93-006

Sutton, S., & Maynard, J. B. (1996). Basement unconformity control on alteration, St. Francois Mountains, SE Missouri. *The Journal of Geology*, *104*(1), 55–70.

Tang, D., Shi, X., Wang, X., & Jiang, G. (2016). Extremely low oxygen concentration in mid-Proterozoic shallow seawaters. *Precambrian Research*, *276*, 145–157. https://doi.org/10.1016/j.precamres.2016.02.005

Tarhan, L., Planavsky, N., Wang, X., Bellefroid, E., Droser, M., & Gehling, J. (2018). The late-stage "ferruginization" of the Ediacara Member (Rawnsley Quartzite, South Australia): Insights from uranium isotopes. *Geobiology*, *16*(1), 35–48. https://doi.org/10.1111/gbi.12262

Toma, J., Holmden, C., Shakotko, P., Pan, Y., & Ootes, L. (2019). Cr isotopic insights into ca. 1.9 Ga oxidative-weathering of the continents utilizing the Beaverlodge Lake paleosol, Northwest Territories, Canada. *Geobiology*. https://doi.org/10.1111/gbi.12342

Utsunomiya, S., Murakami, T., Nakada, M., & Kasama, T. (2003). Iron oxidation state of a 2.45-Byr-old paleosol developed on mafic volcanics. *Geochimica et Cosmochimica Acta*, *67*(2), 213–221.

Wallace, M. W., Hood, A. V. S., Shuster, A., Greig, A., Planavsky, N. J., & Reed, C. P. (2017). Oxygenation history of the Neoproterozoic to early Phanerozoic and the rise of land plants. *Earth and Planetary Science Letters*, *466*, 12–19. https://doi.org/10.1016/j.epsl.2017.02.046

Wang, X., Planavsky, N. J., Reinhard, C. T., Zou, H., Ague, J. J., Wu, Y., … Peucker-Ehrenbrink, B. (2016). Chromium isotope fractionation during subduction-related metamorphism, black shale weathering, and hydrothermal alteration. *Chemical Geology*, *423*, 19–33. https://doi.org/10.1016/j.chemgeo.2016.01.003

Watanabe, Y., Martini, J. E., & Ohmoto, H. (2000). Geochemical evidence for terrestrial ecosystems 2.6 billion years ago. *Nature*, *408*(6812), 574–578.

Wille, M., Babechuk, M. G., Kleinhanns, I. C., Stegmaier, J., Suhr, N., Widdowson, M., … Schoenberg, R. (2018). Silicon and chromium stable isotopic systematics during basalt weathering and lateritisation: A comparison of variably weathered basalt profiles in the Deccan Traps, India. *Geoderma*, *314*, 190–204. https://doi.org/10.1016/j.geoderma.2017.10.051

Wilson, A. H., & Zeh, A. (2018). U-Pb and Hf isotopes of detrital zircons from the Pongola Supergroup: Constraints on deposition ages, provenance and Archean evolution of the Kaapvaal craton. *Precambrian Research*, *305*, 177–196.

Zbinden, E., Holland, H., Feakes, C., & Dobos, S. (1988). The Sturgeon Falls paleosol and the composition of the atmosphere 1.1 Ga BP. *Precambrian Research*, *42*(1–2), 141–163. https://doi.org/10.1016/0301-9268(88)90014-9

Zhang, S., Wang, X., Wang, H., Bjerrum, C. J., Hammarlund, E. U., Costa, M. M., … Canfield, D. E. (2016). Sufficient oxygen for animal respiration 1,400 million years ago. *Proceedings of the National Academy of Sciences of the United States of America*, *113*(7), 1731–1736. https://doi.org/10.1073/pnas.1523449113

Zhang, S., Wang, X., Wang, H., Hammarlund, E. U., Su, J., Wang, Y., & Canfield, D. E. (2017). The oxic degradation of sedimentary organic matter 1400 Ma constrains atmospheric oxygen levels. *Biogeosciences*, *14*(8), 2133.

Zhao, M., Reinhard, C. T., & Planavsky, N. (2017). Terrestrial methane fluxes and Proterozoic climate. *Geology*, *46*(2), 139–142. https://doi.org/10.1130/G39502.1

SUPPORTING INFORMATION

Additional supporting information may be found online in the Supporting Information section at the end of the article.

How to cite this article: Colwyn DA, Sheldon ND, Maynard JB, et al. A paleosol record of the evolution of Cr redox cycling and evidence for an increase in atmospheric oxygen during the Neoproterozoic. *Geobiology*. 2019;00:1–15. https://doi.org/10.1111/gbi.12360